Estimating Paleointensities From Chemical Remanent Magnetizations of Magnetite Using Non-Heating Methods

C. Maurel, J. Gattacceca

JGR Planets

RESEARCH ARTICLE
10.1029/2023JE007779

Estimating Paleointensities From Chemical Remanent Magnetizations of Magnetite Using Non-Heating Methods

C. Maurel[1] **and J. Gattacceca**[1]

[1]CNRS, Aix Marseille University, IRD, INRAE, CEREGE, Aix-en-Provence, France

Key Points:

- We determine empirical coefficients relating a measured chemical remanent magnetization (CRM) and the magnetizing field intensity
- The coefficients differ by a factor of ~3 from those used in previous studies and adapted to samples with thermoremanent magnetization
- Published lower limits on CRM paleointensities from magnetite-bearing meteorites can be revised and new data more accurately interpreted

Supporting Information:

Supporting Information may be found in the online version of this article.

Correspondence to:

C. Maurel,
cmaurel@cerege.fr

Citation:

Maurel, C., & Gattacceca, J. (2023). Estimating paleointensities from chemical remanent magnetizations of magnetite using non-heating methods. *Journal of Geophysical Research: Planets*, *128*, e2023JE007779. https://doi.org/10.1029/2023JE007779

Received 8 FEB 2023
Accepted 31 MAY 2023
Corrected 27 JUL 2023

This article was corrected on 27 JUL 2023. See the end of the full text for details.

Author Contributions:

Conceptualization: C. Maurel, J. Gattacceca
Data curation: C. Maurel
Formal analysis: C. Maurel
Investigation: C. Maurel, J. Gattacceca
Methodology: C. Maurel, J. Gattacceca
Writing – original draft: C. Maurel
Writing – review & editing: C. Maurel, J. Gattacceca

Abstract Many meteorites experienced aqueous alteration on their parent body. During this process, magnetite usually forms and acquires a chemical remanent magnetization (CRM) if growing in the presence of a magnetic field. The epoch of aqueous alteration on planetesimals encompasses the lifetime of the solar nebula. Therefore, magnetite-bearing meteorites are potential sources of invaluable data regarding the intensity of the solar nebula magnetic field and its influence on planetary accretion. The major limitation encountered in meteorite paleomagnetic studies is the lack of an empirical law relating a CRM characterized using non-heating methods and the magnetizing field intensity. This issue is usually bypassed using the empirical law for non-heating methods calibrated for thermoremanent magnetizations (TRM), resulting in poorly constrained paleointensities. Here, we determine such an empirical law through a series of CRM acquisition experiments. Magnetite is grown in weakly magnetic sedimentary rocks and synthetic samples in a magnetic field while heated at 350°C for 5 hr in an argon atmosphere. All samples exhibit a high-coercivity magnetization parallel and proportional to the field applied, identified as a CRM carried by magnetite. We determine the CRM empirical law by retrieving the applied field intensity using non-heating methods. The empirical coefficients differ from the TRM ones by a factor of 1.9–3.2 depending on the method. We use these coefficients to revisit the paleointensities published for the CM chondrite Murchison and the C2 ungrouped Tagish Lake. This empirical law opens the door to the study of numerous magnetite-bearing meteorites potentially carrying a CRM.

Plain Language Summary Meteorites provide us with invaluable clues to understand the origin of our solar system. In particular, some meteorites carry a record of ancient magnetic fields they experienced in the form of a natural remanent magnetization. Magnetic fields sustained in protoplanetary disks may play an essential role in the formation of planetary bodies. The remanent magnetization of some meteorites can therefore inform us of the intensity and longevity of such magnetic fields in our own sun's protoplanetary disk, providing us with precious constraints for models of planetary formation. In a vast number of meteorites, magnetization is acquired by minerals that form when the rock undergoes alteration during contact with fluids. However, as of today, the relationship between such magnetization measured in the laboratory and the intensity of the ancient field that imparted it is poorly known. In this work, we conduct a series of experiments to determine an empirical law relating these quantities. This law can be used in future meteorite paleomagnetic studies. We also revise the intensities previously estimated for the CM chondrite Murchison (from >2 μT to 2.7 ± 1 μT) and the C2 ungrouped Tagish Lake (from <0.3 μT to <0.9 ± 0.3 μT).

1. Introduction

Many meteorites show petrographic evidence for ancient low-temperature aqueous alteration (Krot et al., 2006). These meteorites include the unequilibrated ordinary chondrites, carbonaceous chondrites from the CM, CO, CI, CV, CK, and CR groups, as well as some ungrouped carbonaceous chondrites. Aqueous alteration is caused by heating primarily due to the decay of ^{26}Al and subsequent melting of water ice accreted on parent bodies. The epoch of aqueous alteration on planetesimals spans the first 15–20 million years (Myr) after the formation of calcium-aluminum-rich inclusions (CAIs) (Krot et al., 2006), but may have occurred mostly within the first ~6 Myr after CAI formation (Vissier et al., 2020). Some meteorite groups also show evidence for pre-accretionary aqueous alteration (Bischoff, 1998). The duration of aqueous alteration is mainly constrained by the availability of water ice and the decay of ^{26}Al (Brearley, 2006; Vissier et al., 2020). During aqueous alteration, the formation of magnetite as a secondary mineral is common, sometimes along with pyrrhotite (Krot et al., 2006). Should it occur in the presence of a magnetic field, the low-temperature formation of these minerals will result in the acquisition of a chemical remanent magnetization (CRM) (Dunlop & Özdemir, 1997). CRM is ubiquitous among terrestrial and extraterrestrial rocks. Unlike thermoremanent magnetization (TRM) acquisition, CRM acquisition

does not require cooling from temperatures above the blocking temperature of the rock's ferromagnetic minerals. Instead, minerals grow beyond their blocking volume and acquire a CRM that reflects the orientation and intensity of the ambient field.

CRMs can be divided into two categories: single-phase CRM and two-phase CRM (Dunlop & Özdemir, 1997). Single-phase CRM defines the cases where the CRM carriers form by pseudomorphosis of a non-magnetic precursor or during precipitation. By contrast, two-phase CRM carriers form out of ferromagnetic precursors that may already carry a remanence. Magnetic exchange coupling between the precursor and new phases may affect the CRM acquisition process and limit the influence of the external field on the produced CRM. Experiments show that, in the case of single-domain grains, the direction of the resulting CRM may be partially inherited from the initial remanence (e.g., Özddemir & Dunlop, 1985, 1989). This appears to break down for larger grains, which are less affected by exchange coupling and therefore more sensitive to external fields (Johnson & Merrill, 1972). However, the influence of the parent mineral's remanence on the intensity of the newly acquired CRM remains largely unknown (Dunlop & Özdemir, 1997). In addition, if new magnetic minerals are forming upon cooling in a magnetic field, they will acquire a so-called thermochemical remanent magnetization (TCRM). A CRM is a TCRM acquired at a constant temperature.

The early epoch of aqueous alteration in meteorites implies that it likely occurred before the dissipation of the solar nebula (~5 Myr after CAI formation) on some parent bodies, and therefore in the presence of the magnetic field sustained by the nebula (Wang et al., 2017; Weiss et al., 2021). Protoplanetary disk fields are increasingly regarded as a prominent acting force during the formation of the first planetary bodies (e.g., Bai, 2016). Complex magnetic effects may enhance angular momentum transport in the disk. This would influence the accretion of solids onto the central star and, as a consequence, favor the formation of planetesimals through the accretion of solid matter (Weiss et al., 2021). Placing constraints on the intensity, spatial and temporal variations of the solar nebula field therefore represents an essential step towards improving our understanding of disk dynamics and planetary formation. In this regard, the numerous meteorites aqueously altered within the lifetime of the nebula offer a unique source of data.

On Earth, because of the abundance of TRM-bearing rocks and the advanced theoretical framework developed to describe TRM acquisition (Dunlop & Özdemir, 1997; Néel, 1955), CRM-bearing samples have been mainly analyzed to obtain directional information on the geomagnetic field (Dunlop & Özdemir, 1997). For meteorites, on the contrary, the direction of the magnetizing field is of limited interest because the samples are unoriented while estimating the paleointensity is crucial. Several paleomagnetic studies have been conducted on aqueously altered meteorites suspected to hold the record of the nebula field as CRMs. Five CM chondrites (Cournède et al., 2015) and the CV chondrite Allende (Carporzen et al., 2011; Fu et al., 2021) were found to carry a natural remanent magnetization (NRM) with a stable, high-coercivity component, interpreted as a record of the solar nebula field. A recent study of samples returned from the asteroid Ryugu by the Hayabusa 2 mission also concluded that they likely carry a substantial CRM acquired in the nebula field. The NRMs of the CO chondrites ALHA77307 and DOM 08006 (Borlina et al., 2022), and the C2 ungrouped Tagish Lake (Bryson et al., 2020) were also characterized as CRM, but estimated paleointensities suggested an acquisition in a weak field or no field. However, in all these studies, the absence of a well-calibrated method to determine paleointensities from the measured CRMs was a major impediment. Because the methods implemented were calibrated for TRM-bearing minerals, the paleointensity estimates were largely uncertain (Nichols, 2021).

The optimal approach to obtain precise paleointensity estimates is to replicate in the laboratory the acquisition of the NRM in a known magnetic field. Samples carrying a TRM are often analyzed using the so-called Thellier-type protocols, which consist of stepwise heating the sample while subjecting it to a known field or zero field alternatively (Coe, 1967; Thellier & Thellier, 1959; Yu et al., 2004). Plotting the NRM remaining against the partial TRM gained at each temperature step provides a direct estimate of the paleointensity. This approach can only be successful, however, if the sample does not alter during heating. Alteration is frequent in meteorite samples, which formed in more reducing conditions than the ones they may experience during the experiments. This challenge can sometimes be overcome by heating in a controlled atmosphere, although success is not guaranteed (Suavet et al., 2014).

Unlike TRM, the acquisition of a CRM cannot be replicated in the laboratory on a CRM-bearing rock because the minerals of interest have already formed. Using TRM methods to determine a paleointensity from a CRM is not optimal: (a) these methods do not reproduce the natural magnetization acquisition process, (b) many samples are susceptible to alteration during heating, and (c) there may be curational constraints precluding heating. Nonetheless, several studies have placed constraints on the CRM to TRM ratio using theory (McClelland, 1996), modeling (Baker

& Muxworthy, 2023) and experiments. These experiments consisted of growing magnetite (Kobayashi, 1959; Pick & Tauxe, 1991; Pucher, 1969) or titanomagnetite (Draeger et al., 2006; Gribov et al., 2019; Maksimochkin et al., 2019; Shcherbakov et al., 2017) in a known magnetic field and comparing it with the TRM acquired in the same magnetic field using Thellier-type methods. It was reported that Arai plots (i.e., NRM lost vs. partial TRM gained) obtained over high-temperature intervals (>400°C) can be used to compare a laboratory TRM to the original CRM to estimate a paleointensity (Draeger et al., 2006; Shcherbakov et al., 2017). This only works in the favorable case where the sample does not significantly alter before reaching these temperatures. In most of these studies, the CRM to TRM ratio was estimated at around 0.5, although a wide spectrum of values was reported, including ratios close to 1.

Alternative methods can be applied to obtain paleointensity estimates without having to heat the sample. These non-heating methods consist of (a) demagnetizing the NRM of the sample using alternating fields (AF), (b) imparting an anhysteretic remanent magnetization (ARM) or saturation isothermal remanent magnetization (sIRM) to the sample and AF-demagnetizing it again, (c) using the slope of the NRM versus ARM or sIRM lost during the demagnetization sequence to estimate the paleointensity following Equations 1 and 2 (Gattacceca & Rochette, 2004; Stephenson & Collinson, 1974).

$$B_{\text{paleo}} = a\frac{d\text{NRM}}{d\text{IRM}} \tag{1}$$

$$B_{\text{paleo}} = \frac{B_{\text{ARM}}}{f}\frac{d\text{NRM}}{d\text{ARM}} \tag{2}$$

In Equations 1 and 2, B_{paleo} is the paleointensity, NRM, ARM, and IRM are stepwise demagnetization data for each of these remanence types and B_{ARM} is the bias field applied during ARM acquisition. a and f are empirical coefficients, which must be accurately determined to obtain reliable paleointensity estimates. A number of experiments were conducted to constrain the value of a and f in the case of a TRM. TRM acquisition by different carriers, including magnetite, was investigated using both natural and synthetic samples for a wide range of grain sizes (Dunlop & Argyle, 1997; Harstra, 1982, 1983; Lerner et al., 2017; Muxworthy & McClelland, 2000; Weiss & Tikoo, 2014; Yu, 2010; Yu & Dunlop, 2003; Yu et al., 2007).

These coefficients remain, however, essentially unknown if the sample's NRM is a CRM. Pick and Tauxe (1991) produced magnetite powder in a known magnetic field by alteration of green rust under reducing conditions and determined the CRM to ARM ratio for various applied fields. This ratio can be used in place of the derivative of the demagnetization sequence in Equations 1 and 2 to calculate the coefficient f. However, using the whole demagnetization sequence produces more accurate paleointensity estimates, in particular for samples carrying multicomponent magnetizations (Gattacceca & Rochette, 2004). Paleomagnetic studies of CRM-bearing meteorites have so far used the values of a and f estimated for TRM-bearing samples to obtain paleointensity estimates. These paleointensities are lower limit estimates, based on the abovementioned studies that compared CRMs to laboratory TRMs and showed that CRM/TRM ratios are <1 (e.g., Draeger et al., 2006). Several recent studies have stressed the importance of better constraining the values of a and f for CRMs (Borlina et al., 2022; Bryson et al., 2020; Nichols, 2021). The objective of our study is to determine these empirical factors in the case of a single-phase CRM carried by magnetite grains. Because most meteorites potentially carrying a CRM experienced very mild heating (<100–150°C), we focus on the acquisition of CRMs and not TCRMs.

We present CRM acquisition experiments where magnetite is grown in natural and synthetic samples heated at 350°C for 5 hr in an argon atmosphere and in the presence of a known magnetic field. The rock magnetic properties of the samples are characterized before and after the experiments. We use the stepwise AF demagnetization data of the NRM, ARM and sIRM of the samples to determine a and f using Equations 1 and 2. Table 1 summarizes the symbols used in this paper.

2. Materials and Methods

2.1. Samples

We selected the following sedimentary rocks based on their low initial abundance in magnetic minerals, indicated by their low saturation magnetization and magnetic susceptibility (Table S1 in Supporting Information S1):

- Callovian-Oxfordian claystone from the Paris basin, drilled near the Bure locality in France (abbreviation: BUR) (Aubourg & Pozzi, 2010).

Table 1
Symbols Used in the Paper

Symbol	Meaning	Symbol	Meaning
a	Empirical CRM factor for the IRM method	hIRM	Demagnetization data of the sIRM applied after 5-hr heating and thermal treatment (Equations 3 and 5)
f	Empirical CRM factor for the ARM method	hARM	Demagnetization data of the ARM applied after 5-hr heating and thermal treatment (Equations 4 and 6)
B_{paleo}	Paleofield (Equations 1 and 2)	a_{meas}	Measured empirical CRM factor for the IRM method (Equations 3 and 5)
B_{ARM}	ARM bias field (Equations 1 and 2)	f_{meas}	Measured empirical CRM factor for the ARM method (Equations 4 and 6)
B_{lab}	Laboratory field (Equation 3)	α	Constant relating true and measured factors a and a_{meas} (Equations 3 and 5)
hRM	Demagnetization data of the total remanence after 5-hr heating experiment (Equation 3)	β	Constant relating true and measured factors f and f_{meas} (Equations 4 and 6)

- Claystone from the Arro-Fiscal Formation of lower to middle Eocene age, drilled near the Sigues locality in France (SIG).
- Callovian-Oxfordian marls from the "Terres Noires" formation of the Southern Subalpine Chain in the French western Alps, collected in the Barles and La Robine localities (BAR and ROB).
- Bioclastic limestone of Priabonian age (late Eocene) from the Issirac lacustrine basin in south-eastern France (ISS) (Lettéron et al., 2022).
- Limestone and dolomites from the Lower Paleozoic Canadian Arctic platform sampled in and around the Haughton impact structure from the Eleanor River formation (HAU3), the Blanley Bay formation (HAU9), and the Bear Point formation (HAU23) (Thorsteinsson & Mayr, 1987).

We also included synthetic samples made of natural pyrite powder with grain size <100 μm dispersed in a plaster matrix (PPY).

2.2. Experimental Setup

Two samples (called *I* and *II*) per lithology were included in each experimental batch. Samples *I*, with masses ranging between ∼2 and ∼8 g, were dedicated to the CRM acquisition, susceptibility measurement and ARM acquisition. Samples *II*, with masses ranging between ∼0.6 and ∼1.4 g, were dedicated to the measurements of intrinsic magnetic properties and IRM acquisition. Remanence measurements were conducted on a 2G-Enterprise SQUID cryogenic magnetometer (model 755R, noise level 5×10^{-12} A m^2) coupled with a 3-axis AF degausser system (100-mT maximum field). The magnetometer is located in a magnetically shielded room with residual field of ∼500 nT. An AGICO AF demagnetizer and anhysteretic magnetizer (model LDA5) were used to impart the ARM. A pulse magnetizer from Magnetic Measurements was used to impart the sIRM. Low-field susceptibility measurements were conducted on an AGICO MFK1 (operating at 200 A m^{-1} and 976-Hz frequency, with a sensitivity of 5×10^{-13} m^3). Hysteresis parameters, IRM acquisition curves and FORC diagrams were acquired on a LakeShore vibrating sample magnetometer (VSM, model 8,300 series). Samples were heated in a controlled-atmosphere ASC Thermal Demagnetizer (model TD48). All measurements were conducted in the Rock Magnetism laboratory at the Centre Européen de la Recherche et de l'Enseignement des Géosciences de l'Environnement (CEREGE, France).

2.2.1. Initial Sample Characterization

Before heating, we measured the low-field susceptibility (χ_{lf}) of samples *I*. We measured and demagnetized their NRM using AF fields of 150 mT. We then imparted an ARM (150 mT AC field and 100 μT DC field), measured and demagnetized again at 150 mT. For one sample per lithology, we stepwise demagnetized the NRM and ARM using AF up to 150 mT. For all samples *II*, we recorded an IRM acquisition in the range 100 μT to 1.5 T, followed by the acquisition of a hysteresis cycle (±1 T field range) to determine the saturation magnetization (M_s), saturation remanent magnetization (M_{rs}), coercive force (B_c) and high-field susceptibility (χ_{hf}). The remanent coercive force (B_{cr}) was determined from a DC backfield experiment. The samples were then subjected to a 3-T field using a pulse magnetizer from Magnetic Measurements. We measured the resulting sIRM with a 2G magnetometer

before demagnetizing the samples at 150 mT. For one sample per lithology, we stepwise demagnetized the sIRM using AF up to 150 mT.

2.2.2. CRM Acquisition Experiment and Analysis

One pair of samples (*I* and *II*) per lithology was heated at 350°C for 5 hr in an argon atmosphere. The temperature, duration and nature of the gas were adjusted during preliminary trials to (a) maximize the amount of secondary ferromagnetic minerals created, (b) minimize further oxidation of these minerals and (c) keep the duration of an experiment within reasonable bounds. We tested the following conditions: (a) 150°C in air for 1 month, (b) 200°C in air for 10 days, (c) 350°C in air for 10 hr, and finally (d) 350°C in argon atmosphere for 5 hr. Conditions (a) and (b) did not produce a significant amount of secondary ferromagnetic minerals. Condition (c) produced abundant secondary ferromagnetic minerals but, in most samples, we noted the presence of a substantial amount of high coercivity minerals, suggesting that the secondary minerals may have further oxidized (e.g., into hematite). We therefore established condition (d) as our nominal protocol.

Throughout the heating phase, the samples were exposed to a controlled magnetic field. We conducted the experiment for five field intensities: 30, 50, 75, 100, and 150 μT, as well as one experiment in zero field (51 samples measured in total). For some lithologies (SIG, BAR, ROB, ISS, and PPY), an additional experiment in zero field was stopped after 45 min to monitor the growth of magnetic minerals. For this, we compared the magnitude of an sIRM acquired before and after the heating. On average, 25 min were needed to reach 350°C inside the furnace. After 5 hr at 350°C, the magnetic field inside the furnace was turned off and the samples were kept at temperature for 20 min, before cooling in zero field down to room temperature during ∼50 min.

The heated samples *I* were stepwise demagnetized using AF up to 150 mT to characterize the acquired remanence (called hRM). We also measured χ_{lf}. We then imparted an ARM to the samples (150-mT AC field, 100-μT DC field). The fact that the samples were left 20 min at 350°C in zero field during the CRM acquisition experiment implies that the acquired remanence was partially thermally demagnetized. Therefore, to accurately compare the demagnetization of the ARM applied after the experiment with that of the hRM, we had to subject the samples to the same thermal treatment after ARM acquisition. To do so, we re-heated the samples at 350°C in an argon atmosphere and zero field after applying the ARM. Samples were kept for 45 min at temperature before cooling. We accounted for 20–25 min for the samples to fully equilibrate at 350°C through their entire volume, such that samples were left at 350°C during 20–25 min, like the CRM. The thermally treated ARM (called hARM) was then demagnetized following the same AF sequence as for the hRM. On samples *II*, we conducted the same rock magnetic measurements as prior heating. The samples were then remagnetized in a 3-T field and their sIRM measured. We applied the same 45-min thermal treatment as the ARM, and stepwise demagnetized the thermally treated sIRM (called hIRM) up to 150 mT following the same sequence as for the hRM.

2.2.3. Transformations Expected Upon Heating

A large number of paleomagnetic and rock magnetic studies describe the complex mineralogical transformations that occur in sedimentary rocks upon heating at various temperatures (Aubourg and Pozzi, 2010; Cairanne et al., 2004; Hirt et al., 1993; Jackson, 1990). These studies show that magnetite primarily forms, in some cases, followed by hematite. In claystone, marls and limestone, both clay minerals and pyrite are sources of the iron needed to form magnetite. Upon oxidation, magnetite can form both by precipitation of fine grains and by pseudomorphosis of pyrite grains, isolated or in framboids (Jackson, 1990; Suk et al., 1993). In both cases, either there is no precursor mineral or the precursor is non-magnetic. This implies that, independently from the formation pathway, the magnetite grains will acquire a single-phase CRM, whose direction and intensity are controlled by the ambient magnetic field and whose stability depends on the size of the secondary minerals (Dunlop & Özdemir, 1997).

2.3. Data Processing

In our experiments, B_{paleo} in Equations 1 and 2 is the field applied in the furnace ($B_{paleo} = B_{lab}$) and the slopes are obtained by applying a linear regression to the demagnetization curves hRM = *f*(hIRM) and hRM = *f*(hARM). However, the quantities hIRM and hARM are the sum of the sIRM or ARM acquired by both the neoformed grains and those originally present. The empirical coefficients determined based on our measurements (a_{meas} and

f_{meas}) are therefore different from the true a and f. If we call $hIRM_{new}$ and $hIRM_{init}$ the fraction of hIRM due to the original and new grains, respectively, we have:

$$B_{lab} = a_{meas}\frac{d\text{hRM}}{d\text{hIRM}} = a_{meas}\frac{d\text{hRM}}{d(\text{hIRM}_{new} + \text{hIRM}_{init})} = a\frac{d\text{hRM}}{d\text{hIRM}_{new}} \quad (3)$$

$$\Longrightarrow a = a_{meas}\left(1 - \frac{d\text{hIRM}_{init}}{d\text{hIRM}}\right)$$

Similarly, we can obtain f from f_{meas}:

$$f = f_{meas}/\left(1 - \frac{d\text{hARM}_{init}}{d\text{hARM}}\right) \quad (4)$$

According to Equations 3 and 4, estimating a and f requires measuring $d\text{hIRM}_{init}/d\text{hIRM}$ and $d\text{hARM}_{init}/d\text{hARM}$, that is, applying to IRM_{init} and ARM_{init} the same thermal treatment as the one applied to IRM and ARM. We did so on unheated samples left over after all other experiments, which included samples of the lithologies SIG, BAR, ROB, ISS and synthetic PPY. We first applied an sIRM or an ARM to the unheated samples and stepwise demagnetized them (up to 100 mT). We then heated the samples for 45 min at 350°C in zero field in an argon atmosphere, before stepwise demagnetizing the thermally treated sIRM ($hIRM_{init}$) or ARM ($hARM_{init}$). Because we could not have these data for all lithologies, we considered re-writing Equation 3 as follows:

$$a = a_{meas}\left(1 - \frac{d\text{hIRM}_{init}}{d\text{IRM}_{init}}\frac{d\text{IRM}_{init}}{d\text{hIRM}}\right) = a_{meas}\left(1 - \alpha\frac{d\text{IRM}_{init}}{d\text{hIRM}}\right) \quad (5)$$

In Equation 5, $d\text{IRM}_{init}/d\text{hIRM}$ is known for all lithologies since we had stepwise demagnetized one unheated sample per lithology (Section 2.2.1), and $\alpha = d\text{hIRM}_{init}/d\text{IRM}_{init}$ is taken as a constant, averaged over all available data (SIG, BAR, ROB, ISS and PPY). Similarly, calling β the average value for $d\text{hARM}_{init}/d\text{ARM}_{init}$:

$$f = f_{meas}/\left(1 - \beta\frac{d\text{ARM}_{init}}{d\text{hARM}}\right) \quad (6)$$

3. Results

3.1. Rock Magnetic Properties and Observable Morphologies

3.1.1. Initial Material

The hysteresis cycles of the unheated samples are dominated by a paramagnetism (for samples BUR, SIG, BAR, ROB, FBL, HAU23) or diamagnetism (for samples ISS, HAU3, HAU9, PPY). The samples exhibit only a weak ferromagnetic contribution, with M_s in the 1.7×10^{-5} to 6.0×10^{-4} A m^2 kg^{-1} range. We find that the M_s values exhibit significant variations within a single lithology (coefficient of variation up to 50%; Table S2 in Supporting Information S1). This indicates some level of heterogeneity in samples from the same lithology. For most samples, the IRM acquisition curve and backfield demagnetization curve are noisy and limited information can be extracted. We also observe variations in low-field susceptibility across lithologies, with mean values between -3.6×10^{-9} m^3 kg^{-1} and 1.0×10^{-7} m^3 kg^{-1} (Table S2 in Supporting Information S1).

For most lithologies, the IRM remaining after the 150-mT demagnetization step represents only ~5% of the initial sIRM, indicating the (quasi) absence of high coercivity minerals. Two exceptions are the HAU3 and HAU23 lithologies, where >50% of the initial sIRM remains at 150 mT. This suggests the presence of very high coercivity grains such as hematite or goethite. However, these grains will have no influence on the outcomes of our experiments for three reasons: (a) the IRM remaining is 10–100 times weaker than the sIRM of the heated samples such that the effect of these grains on the rock magnetic analyses of heated samples will be negligible; (b) the unheated sIRM barely demagnetizes beyond 80 mT, indicating that the coercivity range does not overlap with the medium coercivity range of interest in our study (Section 3.1.2); (c) these high coercivity grains are neither expected to further oxidize and contribute to the CRM nor to carry a pTRM, TCRM or a TVRM given our experimental protocol.

Scanning electron microscope (SEM) images of unheated samples show the presence of framboidal and euhedral pyrites (Figure S1 in Supporting Information S1). Framboidal pyrite is particularly abundant in claystone and

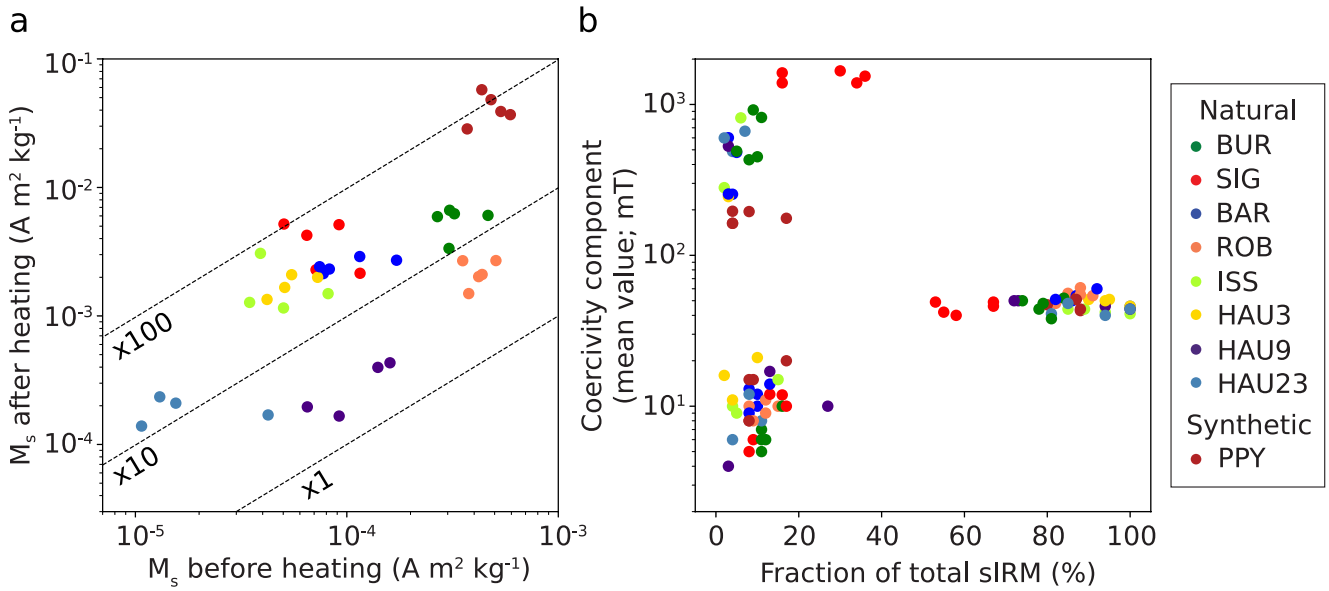

Figure 1. Rock magnetic properties of heated samples. (a) Saturation magnetization (M_s) measured after the chemical remanent magnetization acquisition experiment for all samples of each specimen, as a function of their initial saturation magnetization. The dashed lines correspond to a factor of 1, 10 and 100 between the final and initial M_s. Labels on the right of the figure apply to both panels. (b) Mean values of the coercivity components identified from IRM acquisition curves, as a function of the fraction of total saturation isothermal remanent magnetization they represent.

marls. As indicated by the magnetic properties, the amounts of ferromagnetic iron oxides in the samples are extremely low such that, accordingly, we could not observe any in the nonheated polished sections.

3.1.2. Heated Material

Ferromagnetic minerals are created in all samples during the experiment. After the first 45 min of heating, we measure an increase in sIRM of 1.5–16 (only measured for lithologies SIG, BAR, ROB, ISS, and PPY; Section 2.2.2; Table S3 in Supporting Information S1). At the end of the 5 hr, depending on the lithology, we measure an increase by a factor of 1.5–100 of the M_s (6.0×10^{-5}–5.8×10^{-2} A m^2 kg^{-1}) and M_{rs} (Figure 1a; Figure 2d; Figure S2 and Table S2 in Supporting Information S1). Finally, after the 45-min thermal treatment of the ARM and sIRM applied to the heated samples to obtain hARM and hIRM (Section 2.2.2), we measure an average increase by a factor of 1.2 of the M_s (Table S4 in Supporting Information S1). However, the new grains contributing to this increase will not be given an ARM or sIRM, such that they will not affect our subsequent analyses.

The coercivity spectra of all samples exhibit a dominant coercivity peak near 40 mT (Figure 1b; Figures 2a and 2b). This peak represents more than 70% of the total sIRM for all samples except SIG samples. Almost all samples present a lower coercivity peak near 10 mT, representing between 2% and 15% of the total sIRM. This coercivity range corresponds to the noisiest part of the IRM acquisition curve; we cannot exclude the possibility that in some cases this low-coercivity peak is an artifact. Finally, in more than half of the samples, we identify a higher coercivity peak from 100 to 1,000 mT (~1,500 mT for the SIG samples) representing <10% of the total sIRM, except for the SIG samples.

The dominant coercivity peak is consistent with the presence of small magnetite grains. Using M_s as a proxy, we estimate magnetite content between 0.6 and 600 ppm. We attribute the low-coercivity peak to larger magnetite grains. The high coercivity peak may be due to the presence of pyrrhotite or, perhaps more likely, hematite. Although a fraction of high-coercivity mineral(s) is already present initially in most samples, a larger fraction must have formed during heating to explain the magnitude of the sIRM acquired. Pyrrhotite cannot carry any remanence after the CRM acquisition experiment because the samples are cooled in zero field above the Curie temperature of pyrrhotite. Moreover, we deem it unlikely that the putative formation of hematite will significantly affect our results for two reasons. First, the high-coercivity fraction of the spectra represents only a small fraction of the sIRM compared to the dominant peak. Second, for all samples, the overlap of the two coercivity peaks is

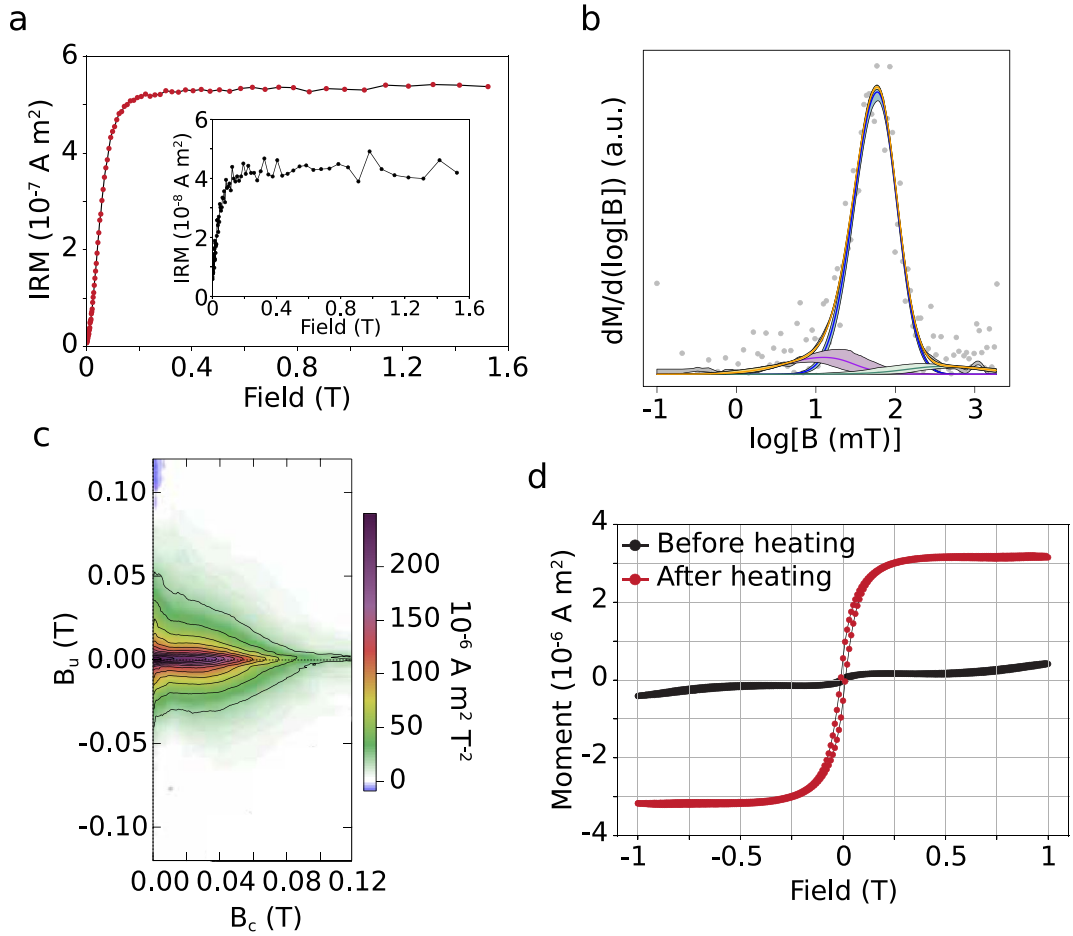

Figure 2. Rock magnetic data set for a sample of the BAR claystone. (a) IRM acquired as a function of field applied after the chemical remanent magnetization acquisition experiment. The inset shows the IRM acquisition curve of the non-heated sample. (b) Coercivity distribution: derivative of the IRM acquisition curve (arbitrary units) as a function of the logarithm of the applied field. Data are shown by the gray points and a spline fit is shown by the gray line (only partially visible). The three coercivity components fitted to the data are shown by the blue, purple and green curves. Shaded areas show the 95% confidence intervals for each curve. The sum of the three coercivity components is shown in orange. This plot was generated using the MAX UnMix software (Maxbauer et al., 2016). (c) First-order reversal curve (FORC) diagram obtained using the FORCinel software (Harrison & Feinberg, 2008). (d) Hysteresis curves of the sample before and after heating.

relatively minor, implying that the medium-coercivity population will dominate the remanence over most of the AF demagnetization range.

On a M_{rs}/M_s versus B_{cr}/B_c plot (Day diagram; Figure S3 in Supporting Information S1), most samples fall in the vortex state (V) region, some fall in the superparamagnetic/single-domain (SP-SD) region (Dunlop, 2002). However, such a diagram can be difficult to interpret in the case of mixtures of different minerals or grain sizes (Roberts et al., 2018). To further investigate the domain state of the created particles, we acquired FORC diagrams for one sample per lithology (Roberts et al., 2014). The diagrams display a variety of patterns (Figure 2c; Figure S4 in Supporting Information S1), which are more complex than the characteristic ones for pure SD, MD or V populations and suggest mixtures of domain states. The different mixtures we identify depending on the lithology are mainly SD-V, although with possible MD or SP contributions (Table S5 in Supporting Information S1).

Finally, in agreement with previous studies (Section 2.2.3) and our rock magnetic findings, SEM images of the samples and electron dispersive spectroscopy analyses show that iron oxides (magnetite) are present in larger quantities in heated samples. They are found in framboidal grains as precipitated grains and pseudomorphic rims around pyrite grains (Figure 3). Note that magnetite SD grains are <100 nm in size, which are abundant in the samples according to the FORC diagrams (Figure S4 in Supporting Information S1), are not observable on regular SEM images.

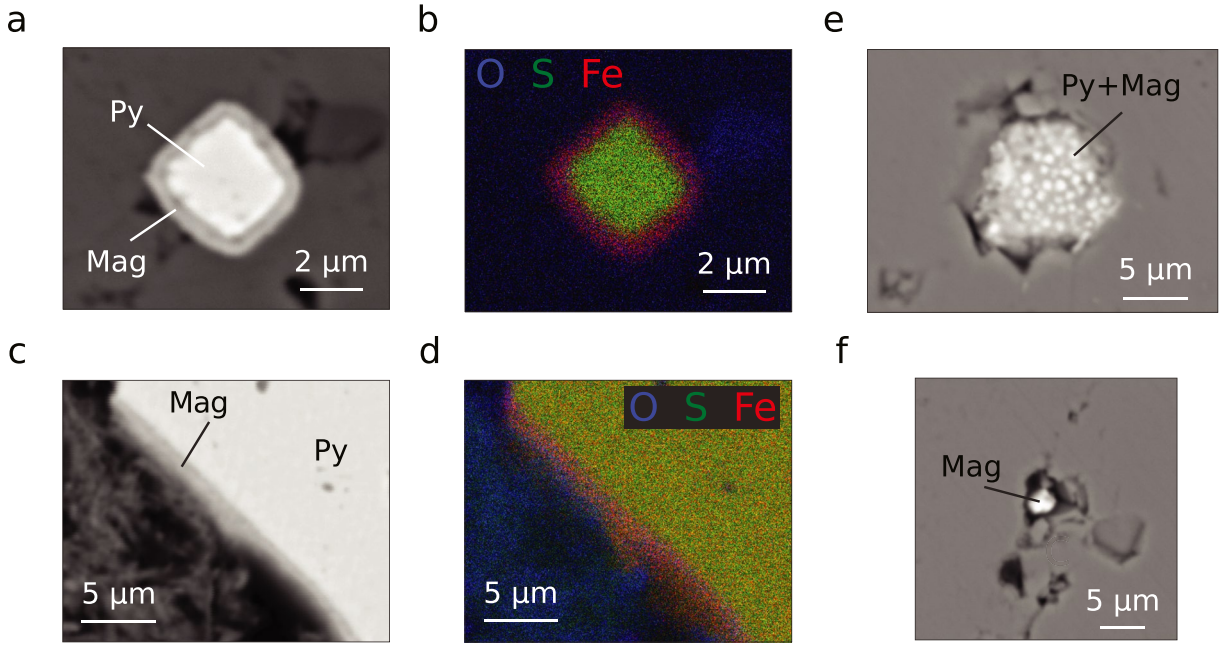

Figure 3. Examples of magnetite morphologies found in heated samples. (a and b) Backscattered electron (BSE) image and corresponding electron dispersive spectroscopy (EDS) map (O, S, Fe) of a pyrite grain (Py) with a magnetite rim (Mag) in the HAU3 lithology. (c and d) BSE image and corresponding EDS map (O, S, Fe) of a large pyrite grain with a magnetite strip in the synthetic sample PPY. (e) Framboidal grains with likely a mixture of pyrite and magnetite. (f) Precipitated magnetite grain in the lithology ISS33.

3.2. Characterization of the Remanence

We conducted five CRM acquisition experiments with different applied field intensities (30, 50, 75, 100, and 150 µT) and one control experiment in zero field. For the zero-field samples, orthogonal projections of the demagnetization data reveal a low-coercivity component ($\lesssim$25 mT; Figure S6 in Supporting Information S1). At higher demagnetization steps, noise dominates the signal. This component could be a consequence of the pre-heating AF demagnetization, putting grains in an unstable configuration of magnetic domain state. In the following, because the coercivity spectra of our samples are dominated by magnetite with peak coercivity ~40 mT (Figure 1b), we focus on the >25-mT portion of the hRM demagnetization data to leave aside potential contaminations in the low coercivity range.

For all samples subjected to a non-zero field, orthogonal projections of the demagnetized hRM exhibit an origin-trending component above 25 mT (Figures 4a–4e). For the samples that could be relatively precisely oriented in the oven, we verify that the high-coercivity component of the hRM is almost parallel to the applied field (average deviation of 6°). The heated samples exhibit degrees of anisotropy $P = 1.11 \pm 0.04$ (1 standard deviation) for both ARM and sIRM (Table S6 in Supporting Information S1). A value of $P = 1.11$ results in a maximum deviation from the applied field direction of 3° (Figure S7 in Supporting Information S1) and a maximum 11% error on the CRM/ARM or CRM/IRM ratios in the worst case scenario where the CRM is acquired along the easy anisotropy axis and the ARM or IRM is given along the hard axis. This is well within the uncertainty of our data and indicates that the magnetic anisotropy of the neoformed carriers does not have a significant effect on our results. Note that our empirical law would need to be reassessed in the case where the formation of secondary minerals results in a strong anisotropy (e.g., pseudomorphosis of a precursor with anisotropic shape distribution, or inheritage of the host rock's structural anisotropy). In addition, the magnitude of the high-coercivity component correlates positively with the intensity of the applied field (Figure 5; Table S7 in Supporting Information S1). As expected, this is not the case for hARM and hIRM (Figure S8 and Table S7 in Supporting Information S1). It is also increasingly well defined as the intensity of the applied field increases (Figures 4a–4e), as illustrated by the decrease of the maximum angular deviation (a quantitative measure of the uncertainty of the recovered direction; Kirschvink, 1980) with applied field intensity (Figure S9 in Supporting Information S1).

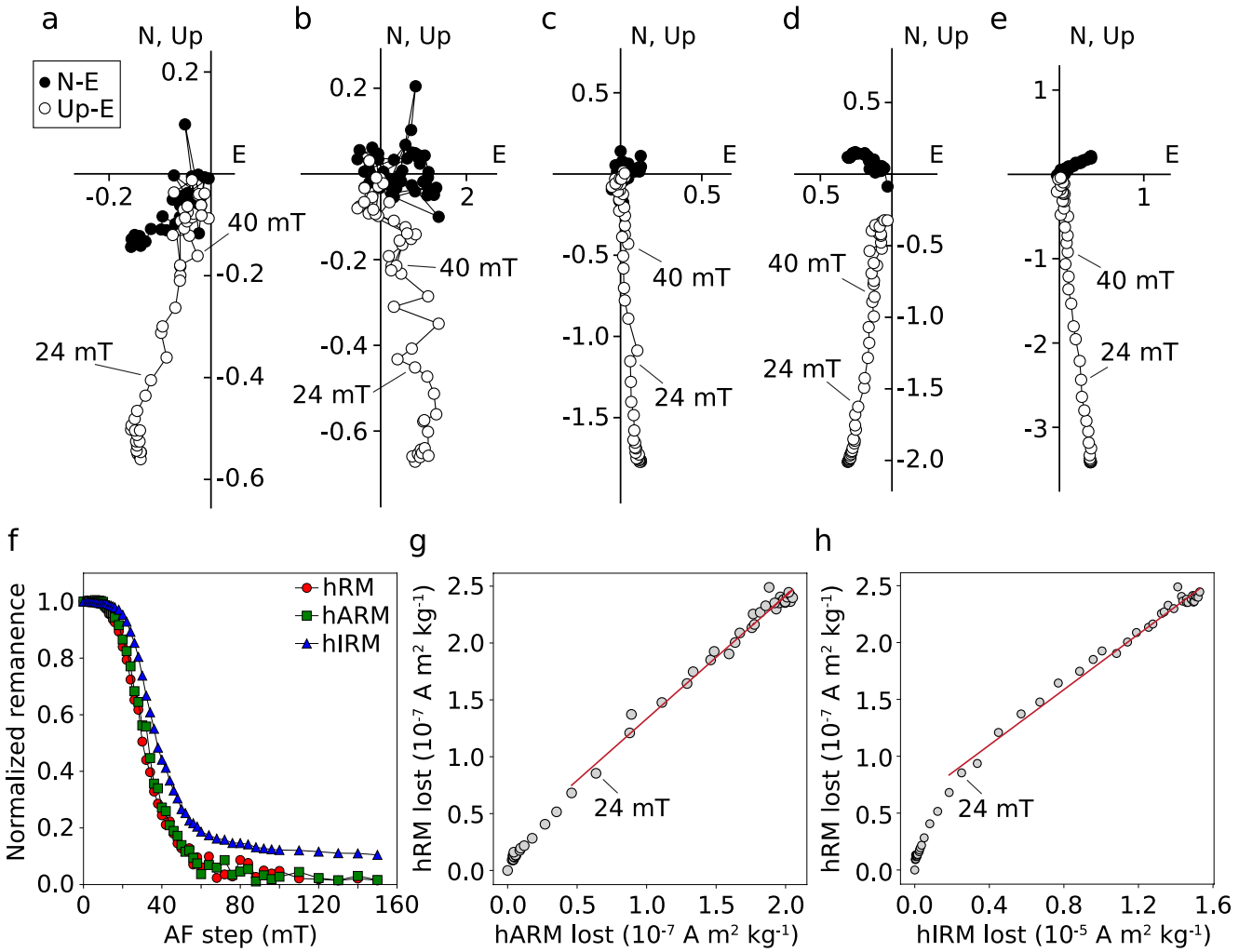

Figure 4. Paleomagnetic data set for samples of the sediment ISS. (a–e) Orthogonal demagnetization plots of the remanence acquired during heating (hRM, in 10^{-9} A m^2) in a field of 30, 50, 75, 100, and 150 μT, respectively. The demagnetization steps range from 0 to 150 mT. (f) Magnetic moment normalized to its initial value measured over the demagnetization sequence of the hRM, hARM and hIRM. If the hRM and hARM curves very closely match, the hIRM curve suggests the presence of a higher (>150 mT) coercivity mineral that is not demagnetized at the end of the sequence. (g and h) hRM lost as a function of hARM (resp. hIRM) lost over the demagnetization sequence. The red line shows the linear regression applied to the >24-mT portion of the curve to obtain dCRM/dhARM (resp. dCRM/dhIRM).

Because the samples were cooled in zero field, we can rule out a pTRM or TCRM acquired upon cooling to explain the origin-trending, high-coercivity component and its positive correlation with applied field intensity. On the other hand, both the minerals present initially in the samples and those created during the experiment likely acquired a thermoviscous remanent magnetization (TVRM) during the experiment. By leaving the samples at 350°C in zero field for 20 min at the end of the 5 hr, we allow for substantial decay of the TVRM given the logarithmic dependence of the TVRM on time. In published CRM-acquisition studies with similar setups and lithologies, the authors estimate that the TVRM contribution is no longer significant if the samples are left at temperature in zero field between 5% and 10% of the time spent in field (Kars et al., 2012). Because, in our experiments, this time represents 7% of the in-field time, we conclude that the dominant contribution to the hRM is a CRM.

3.3. Empirical Relationship Between CRM and Paleointensity

For a majority of samples, the high coercivity component of the hRM forms a straight line when plotting hRM lost versus hARM or hIRM lost during AF demagnetization (e.g., Figures 4g and 4h). We could always calculate

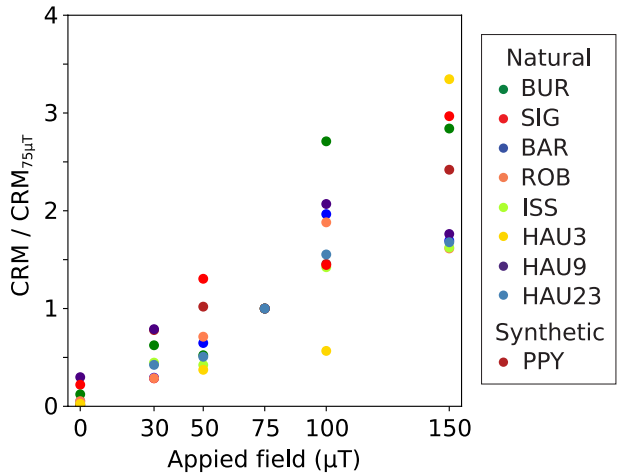

Figure 5. Chemical remanent magnetization (CRM) acquired during the experiments. The CRM, that is, the high-coercivity component of the hRM, is plotted as a function of the intensity of the field applied in the furnace and is normalized by its value for a 75-μT field.

a statistically significant slope on the high-coercivity segment. A linear regression on this segment provides the values for dCRM/dhARM and dCRM/dhIRM (Table S7 in Supporting Information S1).

We call f_{CRM} and a_{CRM} the empirical coefficients f and a estimated in this study. To solve Equation 5 and 6 for f_{CRM} and a_{CRM}, we must determine the values of α, β, $d\text{hIRM}_{init}/d\text{hIRM}$ and $d\text{hARM}_{init}/d\text{hARM}$ (Equations 5 and 6). The two derivatives are obtained by applying a linear regression to the curves $\text{IRM}_{init} = f(\text{hIRM})$ and $\text{ARM}_{init} = \text{f(hARM)}$. As a reminder, IRM_{init} and ARM_{init} are the demagnetization data for the IRM and ARM applied to the unheated samples. The coefficients α and β are average values of $d\text{hIRM}_{init}/d\text{IRM}_{init}$ and $d\text{hARM}_{init}/d\text{ARM}_{init}$, respectively (Section 2.3). We have $\alpha = 0.424 \pm 0.125$ (2 standard error (s.e.)) and $\beta = 0.660 \pm 0.129$ (2 s.e.). The uncertainty on α and β are taken into account in the uncertainty estimate of a_{CRM} and f_{CRM}.

The distributions of the f_{CRM} and a_{CRM} values can be fitted with lognormal probability density functions (Figure 6; Table S7 and S8 in Supporting Information S1). These distributions include all samples for each lithology (as opposed to one sample per lithology) to increase statistical significance. Doing so, we find arithmetic means $f_{CRM} = 1.17 \pm 0.24$ (2 s.e.) and $a_{CRM} = 4{,}001 \pm 862$ μT (2 s.e.). The geometric means for f_{CRM} and a_{CRM} are 0.99 and 3,269, respectively (Table S9 in Supporting Information S1). We find no correlation between the values of the coefficients and the hysteresis parameters of the samples (Figure S10 in Supporting Information S1). We note that the synthetic samples PPY have f_{CRM} values that are twice as large as all the other samples (Figure S10 and Table S7 in Supporting Information S1). We suspect the f_{CRM} may be influenced by the strong magnetostatic interactions revealed by the FORC diagram of PPY samples (Figure S4 in Supporting Information S1).

The arithmetic mean value of f_{CRM} is lower by a factor of 3.2 compared to that of the TRM coefficients compiled from the literature for natural and synthetic samples containing SD/PSD magnetite grains: $f_{TRM} = 3.76 \pm 0.44$ (2 s.e., $N = 142$), while the arithmetic mean value of a_{CRM} is 1.9 times higher: $a_{TRM} = 2{,}067 \pm 308$ μT (2 s.e., $N = 106$) (Figure 6; Table S9 in Supporting Information S1). Lower-limit paleointensities estimated from CRM-bearing samples using TRM coefficients will therefore be underestimated by these factors (Section 4.2).

Our results are in agreement with other studies that estimated the CRM/TRM ratio using theoretical considerations and Thellier-type heating experiments. From Equation 1, an estimate of the CRM/TRM ratio is given by a_{TRM}/a_{CRM} or f_{CRM}/f_{TRM}. We find average values of 0.53 and 0.31, respectively. These values broadly match the ranges estimated from most recent CRM acquisition experiments on titanomagnetites, for example, 0.36–0.90

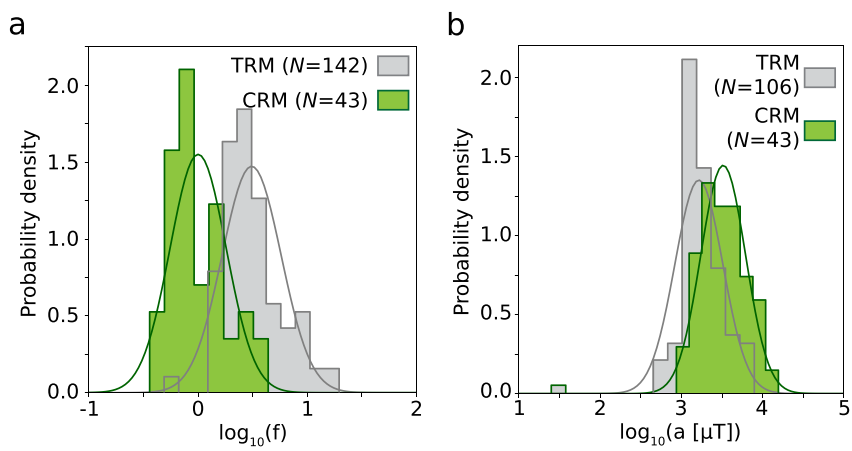

Figure 6. Distributions of the f and a coefficients. (a) Log_{10} of the f_{CRM} coefficients obtained in this study for all samples (green). The gray histogram shows the database of f_{TRM} for magnetite compiled from the literature. Lognormal fits to the data are shown. (b) Same figure as (a) for a_{CRM} and a_{TRM}.

at temperatures of 400–600°C (Draeger et al., 2006), 0.43–0.60 at 400–600°C (Sherbakov et al., 2017); 0.29–0.56 at 350–500°C (Gribov et al., 2019). They are also in overall agreement with the theoretical and modeled ranges for the CRM/TRM ratio of magnetite of 0.34–1.22 (if measured in the temperature range 400–555°C; McClelland, 1996) and ∼0.4 (if measured above 540°C; Baker & Muxworthy, 2023).

4. Discussion

4.1. Relevance to Meteorite Studies

Our experiments reproduce the acquisition of a single-phase CRM by magnetite grains, formed either by precipitation or by pseudomorphosis of a non-magnetic precursor. Because there is no influence of the precursor on the acquired CRM, the CRM direction and intensity are controlled by the magnetizing field and the stability of the CRM depends on the size of the neoformed grains. The empirical relationships that we derive from our results therefore apply to samples hosting magnetite grains in the SD-V magnetic state and carrying a single-phase CRM.

In meteorites, single-phase CRM acquisition can occur when magnetite forms at the expense of Fe-sulfides (troilite). Magnetite with plaquette or framboidal morphology has been associated with this transformation, and is found in at least CI chondrites, CR chondrites, some CM chondrites (Rubin & Ma, 2021), the C2-ungrouped chondrites Tagish Lake and WIS 91600, and samples returned from the asteroid Ryugu (Brearley, 2006; Harju et al., 2014; Sato et al., 2022; Sridhar et al., 2021). Framboidal magnetite in Tagish Lake may also have formed by precipitation (Kimura et al., 2013). FORC diagrams of CI chondrites, WIS 91600 (Sridhar et al., 2021), Tagish Lake (Bryson et al., 2020) and Ryugu (Sato et al., 2022) exhibit a pattern associated with weakly interacting V-MD grains, which resembles that of the ISS and HAU3 lithologies. In the latter lithology, we also find framboidal structures, although we cannot be certain that the magnetite grains dominating the FORC signal are those forming from pyrite framboids.

Another common pathway for magnetite formation in meteorites is the replacement of Fe-Ni metal or to a lesser extent Fe-Ni carbides. In CM, CV and CO chondrites, it produces individual grains of magnetite or magnetite rims around metal grains. FORC diagrams of CM chondrites exhibit patterns typical of SD grains and SD-V mixtures (Sridhar et al., 2021) that resemble those of the lithologies SIG, BUR, and ROB. In these meteorites, magnetite is formed out of a ferromagnetic mineral that may already carry a substantial remanence, which would result in a two-phase CRM. Metal grains in the matrix of unheated chondrites are not expected to carry a uniform remanence because their NRM is acquired upon cooling in the solar nebula and would have been randomized during accretion. This was suggested by Borlina et al. (2022) to explain the absence of substantial magnetization in the matrix of CO chondrites. Following the same reasoning, if a meteorite is found to carry a two-phase CRM uniform across mutually oriented samples, this implies that either the precursor metal was not magnetized or its remanence had a negligible effect on the acquired CRM. In this case, the empirical relationship between CRM and paleointensity determined in this study should remain valid and provide a reliable paleointensity estimate. However, further investigations are needed to address the case of two-phase CRMs.

Pyrrhotite is another common ferromagnetic mineral that may carry a CRM acquired upon pseudomorphosis of troilite (i.e., single-phase CRM). It was identified as the main carrier of the remanence in some CM chondrites and the CV chondrite Allende (Carporzen et al., 2011; Cournède et al., 2015). Our experiments were not designed to study the acquisition of CRM by pyrrhotite but might provide an acceptable approximation for paleointensity estimates because we investigated single-phase CRM acquisition. Experiments dedicated to the CRM acquisition by pyrrhotite are also needed.

4.2. Implications for Published Paleointensities

Several paleomagnetic studies were conducted on aqueously altered meteorites. These studies used non-heating ARM and/or IRM methods with empirical coefficients calibrated for TRMs to provide paleointensity estimates. As such, these estimates are only lower limits and therefore poorly constrained. Magnetite was identified as the main remanence carrier in the CM chondrite Murchison (Cournède et al., 2015), the CO chondrites DOM 08006 and ALHA77307 (Borlina et al., 2022), the C2 ungrouped Tagish Lake (Bryson et al., 2020), and in Ryugu samples (Sato et al., 2022). Tagish Lake and Ryugu samples contain magnetite framboids and may therefore carry a single-phase CRM. The CO chondrites contain metal grains altered to magnetite and may therefore carry a

two-phase CRM. Murchison contains both altered metal grains and framboidal magnetite (Rubin & Ma, 2021). In the case of Murchison, the magnetization is found to be homogenous across mutually oriented samples (Cournède et al., 2015), which implies that either the metal precursor was not magnetized or that its influence on the secondary magnetite was negligible. This reasoning may not hold for the CO chondrites, which were found to carry a very weak remanence (Borlina et al., 2022). In the following, we use our CRM empirical factors to revisit the paleointensities estimated for Tagish Lake and Murchison. We choose to leave aside Ryugu samples as we consider that more work is needed to confidently reject the hypothesis that the samples were remagnetized during return or handling (Sato et al., 2022).

4.2.1. C2 Ungrouped: Tagish Lake

Tagish Lake shows evidence for substantial aqueous alteration with peak metamorphic temperatures <150°C (Herd et al., 2011) and contains framboidal magnetite (Kimura et al., 2013; Rubin & Ma, 2021; Sridhar et al., 2021). The alteration of the parent body likely occurred shortly after its accretion, ∼3–4 Myr after CAI formation (Bryson et al., 2020). Tagish Lake could therefore have recorded a CRM in the presence of the solar nebula field. The AF demagnetization of the NRM does not reveal a clear high-coercivity component despite the abundance of potential remanence carriers (Tagish Lake contains 10 wt.% of magnetite). Bryson et al. (2020) therefore considered the lowest ARM bias field applied to their samples to be an upper bound on the magnetic field experienced by the meteorite. Using $f_{\mathrm{TRM}} = 3.33$, they estimated that Tagish Lake experienced a magnetic field <0.3 μT, implying the meteorite formed beyond 13 astronomical units (au) of the Sun. This upper bound was poorly constrained because determined using f_{TRM}. Using the arithmetic mean of f_{CRM}, this upper bound becomes 0.9 ± 0.3 μT. According to the model proposed by Bryson et al. (2020), a 0.9-μT solar nebula field active 3–4 Myr after CAI formation corresponds to a formation distance of >5 au for Tagish Lake. This remains more distal than most meteorite groups (<4 au) but might no longer require a formation beyond the early orbit of Saturn as originally proposed.

4.2.2. CM Chondrite: Murchison

Murchison shows evidence for aqueous alteration dated at 2.4 ± 0.1 Myr after CAI formation (Pravdivtseva et al., 2013). Thermal demagnetization of Murchison's NRM shows that magnetite is the dominant remanence carrier (Cournède et al., 2015). The NRM exhibits an origin-trending, high-coercivity component upon AF-demagnetization up to 110 mT and thermal demagnetization up to 590°C and is homogenous at least up to the cm scale across mutually oriented samples. Given that Murchison was never heated above 40°C on its parent body, this NRM was identified as a CRM. Using the non-heating IRM method and a value of $a_{\mathrm{TRM}} = 3{,}000$ μT, the authors estimated that Murchison experienced a field intensity that was more intense than 2 μT (accounting for the uncertainty on the orientation of the parent body's rotation axis with respect to the magnetizing field direction; Fu et al., 2014). The consensus is now that this NRM corresponds to a record of the solar nebula field (Bryson et al., 2020). Replacing the arithmetic mean of a_{TRM} with a_{CRM}, the estimate of the solar nebula field at 2.4 ± 0.1 Myr after CAI formation changes from >2 μT to the value of 2.7 ± 1 μT.

5. Conclusions

We conducted a series of CRM acquisition experiments to determine an empirical relationship between a measured single-phase CRM carried by magnetite and the magnetizing field intensity using non-heating ARM and IRM methods. Samples of 10 different lithologies (mostly sedimentary rocks containing clays and sulfides) with a low ferromagnetic mineral content were heated in an argon atmosphere at 350°C for 5 hr in a known magnetic field, before being cooled in zero field. The post-heating rock magnetic characterization indicates that magnetite grains formed in all samples and cover a range of magnetic states from a single domain to vortex state, with a possible contribution of multidomain grains in some samples. The magnitude of the CRM acquired by all samples is proportional to the intensity of the field applied and aligned with the applied field direction. After applying an ARM (resp. IRM) and demagnetizing the samples, we determine the empirical factor f_{CRM} (resp. a_{CRM}) needed to relate these data to the intensity of the magnetizing field. We find that the arithmetic mean value for f_{CRM} (resp. a_{CRM}) is 3.2 (resp. 1.9) times lower (resp. greater) than the value determined for a TRM acquisition. This indicates that the lower-limit paleointensities published for magnetite-bearing meteorites carrying a CRM are underestimated, and we propose revised estimates for the CM chondrite Murchison and the C2 ungrouped Tagish Lake. This work has important implications for future paleomagnetic studies. Aqueously altered meteorites are one of

our principal sources of data regarding the solar nebula field. Placing constraints on the intensity and longevity of this field is a necessary step toward a better understanding of the influence of magnetic fields on planetary accretion. This work also applies to returned extraterrestrial material, such as samples of the asteroids Ryugu and Bennu, as well as the drill cores from Jezero Crater that will be returned by the Mars Sample Return mission.

Conflict of Interest

The authors declare no conflicts of interest relevant to this study.

Data Availability Statement

All data needed to evaluate the conclusions in the paper can be found on the Zenodo repository (Maurel & Gattacceca, 2023).

Acknowledgments
We thank Dr. Y. Yu and an anonymous reviewer for their fruitful comments. We thank Prof. Charles Aubourg for providing the BUR and SIG samples, Prof. Pierre Rochette for fruitful discussions of the results, and Dr. François Demory for assistance during the experiments and for providing the ISS samples. This project received funding from the European Union's Horizon 2020 research and innovation programme under the Marie Skłodowska-Curie grant agreement No. 101027092.

References

Aubourg, C., & Pozzi, J.-P. (2010). Toward a new <250°C pyrrhotite-magnetite geothermometer for claystones. *Earth and Planetary Science Letters*, *294*(1–2), 47–57. https://doi.org/10.1016/j.epsl.2010.02.045

Bai, X.-N. (2016). Towards a global evolutionary model of protoplanetary disks. *The Astrophysical Journal*, *821*(2), 80. https://doi.org/10.3847/0004-637x/821/2/80

Baker, E. B., & Muxworthy, A. R. (2023). Using Preisach theory to evaluate chemical remanent magnetization and its behavior during Thellier-Thellier-Coe paleointensity experiments. *Journal of Geophysical Research: Solid Earth*, *128*(2). https://doi.org/10.1029/2022jb025858

Bischoff, A. (1998). Aqueous alteration of carbonaceous chondrites: Evidence for preaccretionary alteration—A review. *Meteoritics and Planetary Science Journal*, *33*(5), 1113–1122. https://doi.org/10.1111/j.1945-5100.1998.tb01716.x

Borlina, C. S., Weiss, B. P., Bryson, J. F. J., & Armitage, P. J. (2022). Lifetime of the outer solar system nebula from carbonaceous chondrites. *Journal of Geophysical Research: Planets*, *127*(7), e2021JE007139. https://doi.org/10.1029/2021JE007139

Brearley, A. J. (2006). The action of water. In D. S. Lauretta & H. Y. McSween, Jr. (Eds.), *Meteorites and the solar system II* (pp. 584–624). University of Arizona Press.

Bryson, J. F. J., Weiss, B. P., Lima, E. A., Gattacceca, J., & Cassata, W. S. (2020). Evidence for asteroid scattering and distal solar system solids from meteorite paleomagnetism. *The Astrophysical Journal*, *892*(2), 1–24. https://doi.org/10.3847/1538-4357/ab7cd4

Cairanne, G., Brunet, F., Pozzi, J.-P., Besson, P., & Aubourg, C. (2004). Magnetic monitoring of hydrothermal magnetite nucleation-and-growth: Record of magnetic reversals. *American Mineralogist*, *88*(8–9), 1385–1389. https://doi.org/10.2138/am-2003-8-923

Carporzen, L., Weiss, B. P., Elkins-Tanton, L. T., Shuster, D. L., Ebel, D. S., & Gattacceca, J. (2011). Magnetic evidence for a partially differentiated carbonaceous chondrite parent body. *Proceedings of the National Academy of Sciences of the United States of America*, *108*(16), 6386–6389. https://doi.org/10.1073/pnas.1017165108/

Coe, R. S. (1967). Paleointensities of the Earth's magnetic field determined from Tertiary and Quaternary rocks. *Journal of Geophysical Research*, *72*(12), 3247–5281. https://doi.org/10.1029/JZ072i012p03247

Cournède, C., Gattacceca, J., Gounelle, M., Rochette, P., Weiss, B. P., & Zanda, B. (2015). An early solar system magnetic field recorded in CM chondrites. *Earth and Planetary Science Letters*, *410*, 62–74. https://doi.org/10.1016/j.epsl.2014.11.019

Draeger, U., Prévot, M., Poidras, T., & Riisager, J. (2006). Single-domain chemical, thermochemical and thermal remanences in a basaltic rock. *Geophysical Journal International*, *166*(1), 12–32. https://doi.org/10.1111/j.1365-246X.2006.02862.x

Dunlop, D. J. (2002). Theory and application of the day plot (Mrs/Ms versus Hcr/Hc): 1. Theoretical curves and tests using titanomagnetite data. *Journal of Geophysical Research*, *107*(B3), 2056. https://doi.org/10.1029/2001JB000486

Dunlop, D. J., & Argyle, K. S. (1997). Thermoremanence, anhysteretic remanence and susceptibility of submicron magnetites: Nonlinear field dependence and variation with grain size. *Journal of Geophysical Research*, *102*(B9), 20199–20210. https://doi.org/10.1029/97JB00957

Dunlop, D. J., & Özdemir, Ö. (1997). In D. Edwards (Ed.), *Rock magnetism: Fundamentals and frontiers* (pp. 367–390). Cambridge University Press.

Fu, R. R., Volk, M. W. R., Bilardello, D., Libourel, G., Lesur, G. R. J., & Ben Dor, O. (2021). The fine-scale magnetic history of the Allende meteorite: Implications for the structure of the solar nebula. *AGU Advances*, *2*(3), e2021AV000486. https://doi.org/10.1029/2021AV000486

Fu, R. R., Weiss, B. P., Lima, E. A., Harrison, R. J., Bai, X.-N., Desch, S. J., et al. (2014). Solar nebula magnetic fields recorded in the Semarkona meteorite. *Science*, *346*(6213), 1089–1092. https://doi.org/10.1126/science.1258022

Gattacceca, J., & Rochette, P. (2004). Toward a robust normalized magnetic paleointensity method applied to meteorites. *Earth and Planetary Science Letters*, *227*(3–4), 377–393. https://doi.org/10.1016/j.epsl.2004.09.013

Gribov, S. K., Shcherbakov, V. P., & Aphinogenova, N. A. (2019). Magnetic properties of artificial CRM created on titanomagnetite-bearing oceanic basalts. In D. Nurgaliev, V. Shcherakov, A. Kosterov, & S. Spassov (Eds.), *Recent advances in rock magnetism, environmental magnetism and paleomagnetism* (pp. 173–194). Springer.

Harju, E., Rubin, A., Ahn, I., Choi, B., Ziegler, K., & Wasson, J. (2014). Progressive aqueous alteration of CR carbonaceous chondrites. *Geochimica et Cosmochimica Acta*, *139*, 267–292. https://doi.org/10.1016/j.gca.2014.04.048

Harrison, R. J., & Feinberg, J. M. (2008). FORCinel: An improved algorithm for calculating first-order reversal curve distributions using locally weighted regression smoothing. *Geochemistry, Geophysics, Geosystems*, *9*(5), Q05016. https://doi.org/10.1029/2008GC001987

Hartstra, R. L. (1982). A comparative study of the ARM and Zsr of some natural magnetites of MD and PSD grain size. *Geophysical Journal of the Royal Astronomical Society*, *71*(2), 497–518. https://doi.org/10.1111/j.1365-246X.1982.tb05999.x

Hartstra, R. L. (1983). TRM, ARM and Isr of two natural magnetites of MD and PSD grain size. *Geophysical Journal of the Royal Astronomical Society*, *73*(3), 719–737. https://doi.org/10.1111/j.1365-246X.1983.tb03342.x

Herd, C. D. K., Blinova, A., Simkus, D. N., Huang, Y., Tarozo, R., Alexander, C. M. O., et al. (2011). Origin and evolution of prebiotic organic matter as inferred from the Tagish Lake meteorite. *Science*, *332*(6035), 1304–1307. https://doi.org/10.1126/science.1203290

Hirt, A. M., Banin, A., & Gehring, A. U. (1993). Thermal generation of ferromagnetic minerals from iron-enriched smectites. *Geophysical Journal International*, *115*(3), 1161–1168. https://doi.org/10.1111/j.1365-246x.1993.tb01518.x

Jackson, M. (1990). Diagenetic sources of stable remanence in remagnetized paleozoic cratonic carbonates: A rock magnetic study. *Journal of Geophysical Research*, *95*(B3), 2753–2761. https://doi.org/10.1029/jb095ib03p02753

Johnson, H. P., & Merrill, R. T. (1972). Magnetic and mineralogical change associated with low-temperature oxidation of magnetite. *Journal of Geophysical Research*, *77*(2), 334–341. https://doi.org/10.1029/JB077i002p00334

Kars, M., Aubourg, C., Pozzi, J.-P., & Janots, D. (2012). Continuous production of nanosized magnetite through low grade burial. *Geochemistry, Geophysics, Geosystems*, *13*(8), Q08Z48. https://doi.org/10.1029/2012GC004104

Kimura, Y., Sato, T., Nakamura, N., Nozawa, J., Nakamura, T., Tsukamoto, K., & Yamamoto, K. (2013). Vortex magnetic structure in framboidal magnetite reveals existence of water droplets in an ancient asteroid. *Nature Communications*, *4*(1), 2649. https://doi.org/10.1038/ncomms3649

Kirschvink, J. L. (1980). The least-squares line and plane and the analysis of palaeomagnetic data. *Geophysical Journal of the Royal Astronomical Society*, *62*(3), 699–718. https://doi.org/10.1111/j.1365-246x.1980.tb02601.x

Kobayashi, K. (1959). Chemical remanent magnetization of ferromagnetic minerals and its application to rock magnetism. *Journal of Geomagnetism and Geoelectricity*, *10*(3), 99–117. https://doi.org/10.5636/jgg.10.99

Krot, A. N., Hutcheon, I. D., Brearley, A. J., Pravdivtseva, O. V., Petaev, M. I., & Hohenberg, C. M. (2006). Timescales and settings for alteration of chondritic meteorites. In D. S. Lauretta & H. Y. McSweenJr. (Eds.), *Meteorites and the solar system II* (pp. 525–553). University of Arizona Press.

Lerner, G. A., Smirnov, A. V., Surovitckii, L. V., & Piispa, E. J. (2017). Nonheating methods for absolute paleointensity determination: Comparison and calibration using synthetic and natural magnetite-bearing samples. *Journal of Geophysical Research: Solid Earth*, *122*, 1614–1633. https://doi.org/10.1002/2016JB013777

Lettéron, A., Hamon, Y., Fournier, F., Demory, F., Séranne, M., & Joseph, P. (2022). Stratigraphic architecture of a saline lake system: From lake depocentre (Alès Basin) to margins (Saint-Chaptes and Issirac basins), Eocene-Oligocene transition, south-east France. *Sedimentology*, *69*(2), 651–695. https://doi.org/10.1111/sed.12920

Maksimochkin, V. I., Grachev, R. A., & Tselebrovskiy, A. N. (2019). Determination of the formation field of artificial CRM and pTRM by the Thellier method at different oxidation stages of natural titanomagnetite. *Izvestiya*, *56*(3), 413–424. https://doi.org/10.1134/S1069351320030040

Maurel, C., & Gattacceca, J. (2023). Estimating paleointensities from chemical remanent magnetizations of magnetite using non-heating methods [Dataset]. Zenodo. https://doi.org/10.5281/zenodo.7828562

Maxbauer, D. P., Feinberg, J. M., & Fox, D. L. (2016). MAX UnMix: A web application for unmixing magnetic coercivity distributions. *Computers & Geosciences*, *95*, 140–145. https://doi.org/10.1016/j.cageo.2016.07.009

McClelland, E. (1996). Theory of CRM acquired by grain growth, and its implications for TRM discrimination and palaeointensity determination in igneous rocks. *Geophysical Journal International*, *126*(1), 271–280. https://doi.org/10.1111/j.1365-246X.1996.tb05285.x

Muxworthy, A. R., & McClelland, E. (2000). Review of the low-temperature magnetic properties of magnetite from a rock magnetic perspective. *Geophysical Journal International*, *140*(1), 101–114. https://doi.org/10.1046/j.1365-246x.2000.00999.x

Néel, L. (1955). Some theoretical aspects of rock-magnetism. *Advances in Physics B*, *4*(14), 191–243. https://doi.org/10.1080/00018735500101204

Nichols, C. I. O. (2021). Using meteorite magnetism to understand the history of our solar system: A decade of progress and upcoming challenges. *AGU Advances*, *2*(3), e00511. https://doi.org/10.1029/2021AV000511

Özddemir, Ö., & Dunlop, D. J. (1985). An experimental study of chemical remanent magnetizations of synthetic monodomain titanomaghemites with initial thermoremanent magnetizations. *Journal of Geophysical Research*, *90*, 11513–11523. https://doi.org/10.1029/JB090iB13p11513

Özdemir, Ö., & Dunlop, D. J. (1989). Chemico-viscous remanent magnetization in the Fe3O4-yFe2O3 system. *Science*, *243*(4894), 1043–1047. https://doi.org/10.1126/science.243.4894.1043

Pick, T., & Tauxe, L. (1991). Chemical remanent magnetization in synthetic magnetite. *Journal of Geophysical Research*, *96*(B6), 9925–9936. https://doi.org/10.1029/91JB00706

Pravdivtseva, O., Meshik, A., & Hohenberg, C. M. (2013). The I-Xe record: Early onset of aqueous alteration in magnetites separated from CM and CV carbonaceous chondrites. *Lunar and Planetary Science Conferance*, *44*.

Pucher, R. (1969). Relative stability of chemical and thermal remanence in synthetic ferrites. *Earth and Planetary Science Letters*, *6*(2), 107–111. https://doi.org/10.1016/0012-821X(69)90127-7

Roberts, A. P., Heslop, D., Zhao, X., & Pike, C. R. (2014). Understanding fine magnetic particle systems through the use of first-order reversal curve diagrams. *Reviews of Geophysics*, *52*(4), 557–602. https://doi.org/10.1002/2014RG000462

Roberts, A. P., Tauxe, L., Heslop, D., Zhao, X., & Jiang, Z. (2018). A critical appraisal of the "Day" diagram. *Journal of Geophysical Research: Solid Earth*, *123*(4), 2618–2644. https://doi.org/10.1002/2017JB015247

Rubin, A., & Ma, C. (2021). Formation of meteoritic minerals on parent bodies. In *Meteorite mineralogy* (pp. 254–316). Cambridge University Press. https://doi.org/10.1017/9781108613767.012

Sato, M., Kimura, Y., Tanaka, S., Hatakeyama, T., Sugita, S., Nakamuna, T., et al. (2022). Rock magnetic characterization of returned samples from asteroid (162173) Ryugu: Implications for paleomagnetic interpretation and paleointensity estimation. *Journal of Geophysical Research: Planets*, *127*(11), e2022JE007405. https://doi.org/10.1029/2022JE007405

Shcherbakov, V. P., Sycheva, N. K., & Gribov, S. K. (2017). Experimental and numerical simulation of the acquisition of chemical remanent magnetization and the Thellier procedure. *Izvestiya*, *53*(5), 645–657. https://doi.org/10.1134/S1069351317040085

Sridhar, S., Bryson, J. F. J., King, A. J., & Harrison, R. J. (2021). Constraints on the ice composition of carbonaceous chondrites from their magnetic mineralogy. *Earth and Planetary Science Letters*, *576*, 117243. https://doi.org/10.1016/j.epsl.2021.117243

Stephenson, A., & Collinson, D. W. (1974). LUNAR magnetic field palaeointensities determined by an anhysteretic remanent magnetization method. *Earth and Planetary Science Letters*, *23*(2), 220–228. https://doi.org/10.1016/0012-821X(74)90196-4

Suavet, C., Weiss, B. P., & Grove, T. L. (2014). Controlled-atmosphere thermal demagnetization and paleointensity analyses of extraterrestrial rocks. *Geochemistry, Geophysics, Geosystems*, *15*(7), 2733–2743. https://doi.org/10.1002/2013GC005215

Suk, D., Voo, R. V. D., & Peacor, D. R. (1993). Origin of magnetite responsible for remagnetization of Early Paleozoic limestones of New York State. *Journal of Geophysical Research*, *98*(B1), 419–434. https://doi.org/10.1029/92jb01323

Thellier, E., & Thellier, O. (1959). Sur l'intensité du champ magnétique terrestre dans le passé historique et géologique. *Annales de Geophysique*, *15*, 285–378.

Thorsteinsson, R., & Mayr, U. (1987). *The sedimentary rocks of Devon Island, Canadian Arctic Archipelago* (Vol. 411, pp. 182–183). Geological Survey of Canada Memoir.

Visser, R., John, T., Whitehouse, M. J., Patzek, M., & Bischoff, A. (2020). A short-lived 26Al induced hydrothermal alteration event in the outer solar system: Constraints from Mn/Cr ages of carbonates. *Earth and Planetary Science Letters*, *547*, 116440. https://doi.org/10.1016/j.epsl.2020.116440

Wang, H., Weiss, B. P., Bai, X.-N., Downey, B. G., Wang, J., Suavet, C., et al. (2017). Lifetime of the solar nebula constrained by meteorite paleomagnetism. *Science*, *355*(6325), 623–627. https://doi.org/10.1126/science.aaf5043

Weiss, B. P., Bai, X.-N., & Fu, R. R. (2021). History of the solar nebula from meteorite paleomagnetism. *Science Advances*, *7*(1), eaba5967. https://doi.org/10.1126/sciadv.aba5967

Weiss, B. P., & Tikoo, S. M. (2014). The lunar dynamo. *Science*, *346*(6214). https://doi.org/10.1126/science.1246753

Yu, Y. (2010). Paleointensity determination using anhysteretic remanence and saturation isothermal remanence. *Geochemistry, Geophysics, Geosystems*, *11*(2), Q02Z12. https://doi.org/10.1029/2009GC002804

Yu, Y., & Dunlop, D. J. (2003). On partial thermoremanent magnetization tail checks in Thellier paleointensity determination. *Journal of Geophysical Research*, *108*(B11), 2523. https://doi.org/10.1029/2003JB002420

Yu, Y., Tauxe, L., & Gee, J. S. (2007). A linear field dependence of thermoremanence in low magnetic fields. *Physics of the Earth and Planetary Interiors*, *162*(3–4), 244–248. https://doi.org/10.1016/j.pepi.2007.04.008

Yu, Y., Tauxe, L., & Genevey, A. (2004). Toward an optimal geomagnetic field intensity determination technique. *Geochemistry, Geophysics, Geosystems*, *5*(2), 1–18. https://doi.org/10.1029/2003gc000630

Erratum

The originally published version of this article contained typographical errors. The tenth sentence of the abstract should read: "The empirical coefficients differ from the TRM ones by a factor of 1.9–3.2 depending on the method." The value in the term present in the last sentence of the Plain Language Summary should read: "(from >2 μT to 2.7 ± 1 μT)." The citation for Table S8 in Supporting Information was incorrectly omitted from the first sentence of the third paragraph of Section 3.3. The third sentence of the third paragraph of Section 3.3 should read: "Doing so, we find arithmetic means f_{CRM} = 1.17 ± 0.24 (2 s.e.) and a_{CRM} = 4,001 ± 862 μT (2 s.e.). The geometric means for f_{CRM} and a_{CRM} are 0.99 and 3,269, respectively (Table S9 in Supporting Information S1)." The first sentence of the fourth paragraph of Section 3.3 should read: "The arithmetic mean value of f_{CRM} is lower by a factor of 3.2 compared to that of the TRM coefficients compiled from the literature for natural and synthetic samples containing SD/PSD magnetite grains: f_{TRM} = 3.76 ± 0.44 (2 s.e., N = 142), while the arithmetic mean value of a_{CRM} is 1.9 times higher: a_{TRM} = 2,067 ± 308 μT (2 s.e., N = 106) (Figure 6; Table S9 in Supporting Information S1)." The values in the third sentence of the fifth paragraph of Section 3.3 should read: "0.53 and 0.31." The beginning of the eighth sentence of Section 4.2.1 should read: "Using the arithmetic mean of f_{CRM}, ..." The last sentence of Section 4.2.2 should read: "Replacing the arithmetic mean of a_{TRM} with a_{CRM}, the estimate of the solar nebula field at 2.4 ± 0.1 Myr after CAI formation changes from >2 μT to the value of 2.7 ± 1 μT." The sixth sentence of the Conclusions should read: "We find that the arithmetic mean value for f_{CRM} (resp. a_{CRM}) is 3.2 (resp. 1.9) times lower (resp. greater) than the value determined for a TRM acquisition." In addition, an error has been fixed in the correction factors needed to calculate the empirical factors f and a in Figure 6 and Table S8 in Supporting Information S1. The corrected mean values are presented. Geometric means of the coefficient distributions have been added to Table S9 in Supporting Information S1. This version may be considered the authoritative version of record.